EFFECT OF SPRAYING PARAMETERS ON THE PEMFCs CATALYST LAYER ARCHITECTURE AND PERFORMANCE

M.V. Sinyakov [1], D.E. Grineva [1], R.M. Mensharapov [1], S.V. Nagornyy [1], T.D. Patsaev [1], V.N. Fateev [1], A.Sh. Aliyev[2], D.D. Spasov [1,3*]

[1]National Research Center "Kurchatov Institute", 1, Akademika Kurchatova sq., 123182 Moscow, Russia
[2]Institute of Chemistry PLE, Ministry of Science and Education of the Republic of Azerbaijan, H. Cavid Ave. 113, AZ 1143, Baku, Azerbaijan
[3]National Research University "Moscow Power Engineering Institute", 14, Krasnokazarmennaya st., 111250 Moscow, Russia
**e-mail: spasovdd@outlook.com*

Received 03.02.2026
Accepted 15.05.2026

Abstract: *Robust methods for fabricating high-quality catalytic layers of membrane-electrode assemblies for PEMFC are crucial for achieving high device efficiency and stability. One of the most common approaches for producing catalytic layers involves spraying catalyst ink onto the surface of a gas diffusion layer or a PEM. This method offers advantages in simplicity, low cost, and accessibility, yet requires thorough parameter optimization to obtain layers with defined morphology, thickness, and porosity. This work investigates the influence of parameters such as catalyst ink composition, suspension feed rate, heating temperature, and airbrush traverse speed. The best performance characteristics were demonstrated by samples with the catalytic layer applied directly onto the PEM at a temperature of at least 40 °C and an ink flow rate not exceeding 54 μl·min^{-1}. However, when depositing onto the GDL, the uniformity of the catalytic layers and the catalyst ink composition were identified as critically important factors.*
Keywords: *PEMFC; gas diffusion layer, membrane-electrode assemblies, catalyst coated membrane, spraying catalyst ink*

1. Introduction

Hydrogen energy is recognized as a key element of the global transition to a low-carbon economy, offering solutions for long-term energy storage and decarbonization of hard-to-abate sectors. Fuel cells (FCs), particularly proton exchange membrane fuel cells (PEMFCs), are of particular importance in this context, enabling highly efficient direct conversion of chemical energy into electricity without harmful emissions [1]. Despite progress in reducing cost, increasing durability, and improving the efficiency of FCs, significant challenges remain in creating high-efficiency catalyst layer (CL) architectures that demonstrate enhanced FC performance [2–15].

The catalyst layer fabrication process affects the distribution of the ionomer and carbon binder network and the formation of the porous structure [16]. In general, the CL formation process can be divided into two main approaches. The first involves forming the layer on the gas diffusion layer (GDL) (gas diffusion electrode (GDE) process), and the second, which is currently the primary method, involves forming it directly on the PEM (catalyst coated membrane (CCM) process) [17–21]. Based on the CL formation method, key directions can be identified, such as the spraying method, slot die coating, brush coating method, dry powder spraying method, screen printing method, sputtering coating, electrochemical deposition, magnetron sputtering, and others [22–34].

The method of spraying catalyst suspension using an airbrush is a manual or semi-automated approach for forming the catalyst layer of PEMFC MEAs. The catalyst ink suspension, containing catalyst, ionomer, and solvent, is delivered under compressed air pressure through the airbrush nozzle, creating a fine aerosol. This aerosol deposits onto the surface of the membrane or gas diffusion layer, forming a uniform thin layer after solvent evaporation. Key advantages of the method are its simplicity of implementation, low equipment cost, and the ability to control layer thickness and coating uniformity. However, achieving reproducible results requires meticulous control of process parameters such as pressure, distance to the substrate, suspension viscosity, and airbrush traverse

speed [35,36]. The air flow rate determines the aerosol dispersion; excessive pressure leads to substrate overwetting, while insufficient pressure causes non-uniform coating. The distance to the substrate directly affects material distribution: too short a distance causes dripping, while excessive distance leads to catalyst loss due to aerosol dispersion. High viscosity hinders spraying, while low viscosity causes component migration and cracking during drying. The airbrush traversal speed determines the layer thickness. Non-uniform movement creates local variations in catalyst density, disrupting mass transport processes in the MEA [37].

The electrostatic spraying method enables the fabrication of MEAs with ultra-low platinum loading (0.01-0.1 $mg \cdot cm^{-2}$), forming a highly dispersed porous catalyst layer structure with enhanced mass transport properties. The best power performance was demonstrated when depositing the catalyst directly onto the membrane (CCM structure) and using catalysts with low Pt content, achieving exceptionally high platinum utilization of up to 56 $kW \cdot g_{pt}^{-1}$. Furthermore, increasing the backpressure to 0.15 MPa enables achieving a peak power density of 0.56 $W \cdot cm^{-2}$ even at a record-low platinum loading of 0.01 $mg \cdot cm^{-2}$ on the cathode [31]. Optimal performance of the membrane-electrode assembly is achieved at a coverage coefficient of k=1.0, which ensures uniform distribution of the catalyst layer. This spraying regime increases peak power by 22.4% compared to k=0.3 and by 11.1% compared to k=3.0, while simultaneously reducing the cathode reaction kinetic resistance by 41% and 27%, respectively. The optimal porous structure formed at k=1.0, with its developed ionomer network, increases the electrochemically active surface area by 16% and promotes the effective formation of triple-phase boundaries [23]. The key parameters determining the quality of catalyst layer spraying are the spray configuration (nozzle path and height) and the catalyst properties, with different batches of Pt/C powders demonstrating different spraying behavior and performance in PEMFCs even with identical ink composition. The use of fresh catalyst is critically important, as powder storage leads to significant power reduction in finished MEAs, and coating uniformity directly depends on mask thickness thinner masks provide better layer uniformity. Modeling the spraying process in MatLAB allows for the optimization of deposition parameters to create catalyst layers with reproducible thickness and maximum performance [22].

The aim of the study was to determine the nature and extent of the influence of the following parameters on the spraying process, and on the thickness and quality of the resulting catalyst layer: the composition of the sprayed catalyst suspension, the airbrush traverse speed, the flow rate of the sprayed substance, and the suspension drying temperature. The study also determined the nature and extent of the influence of catalyst suspension drying parameters on the properties of the PEM during spraying. Furthermore, electrochemical studies were conducted on catalyst layers produced by spraying catalyst suspension onto the surface of electrodes and the PEM.

2. Materials and Methods

2.1. Preparation of catalyst inks and substrates. The catalyst ink for fabricating CLs for PEMFCs consisted of three main components: catalyst, solvent, and an aqueous ionomer solution (Nafion® D1021CS, DuPont, USA). A standard platinum catalyst Pt^{40}/C^{10} was used as the catalyst (Pt content – 40 wt.%, PTFE hydrophobic agent content – 10 wt.%, C – carbon black (Vulcan XC-72, Cabot Corporation, USA). A water-alcohol solution was used as the solvent. The ionomer content in the catalyst ink was 10 wt.%. The suspension for spraying was prepared by mixing all components in the required proportion in a beaker. The beaker's contents were then homogenized using ultrasound (BANDELIN SONOPULS mini20, Germany) for 30 minutes [38].

As substrate for spraying GDL and PEM were used. A Sigracet® 39 BC carbon paper (SGL Carbon, Germany) with a microporous layer and a total thickness of 325 μm was used as the GDL, and a 50-μm-thick Nafion® 212 membrane (DuPont, Wilmington, DE, USA) in the H^+-form was used as the PEM.

2.2. Spraying setup. For directed heating of the GDL and CL surface, a 250 W infrared (IR) quartz electric heater with a heating area of 5×6 cm^2 was used. The heater is installed on the moving

part of the spraying system behind the airbrush and is directed towards the catalyst ink spraying area (Fig. 1b).

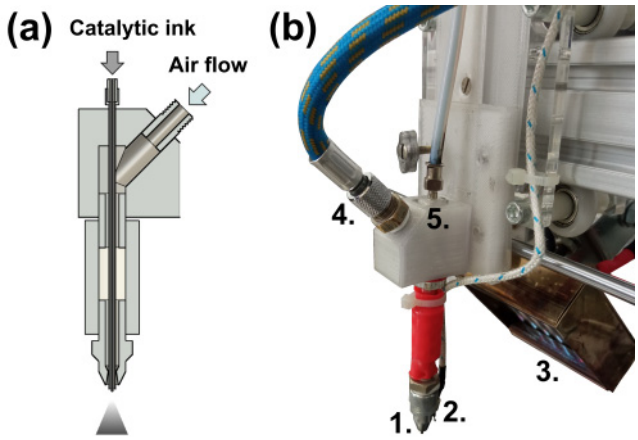

Fig. 1. Schematic diagram of catalyst ink supply and spraying (a); photo of the moving part of the automated spraying system (b). 1 – nozzle, 2 – thermocouple, 3 – IR heater, 4 – air supply hose, 5 – catalyst ink supply needle.

Temperature regulation was carried out using a dimmer. A thermocouple was used to monitor the temperature above the spraying area, with a temperature recording accuracy of ±0.5 °C. A microcontroller board (Arduino) was used for temperature recording and setting the heating temperature in real time. Maintaining the set temperature was performed automatically using a PID controller algorithm.

Ink delivery to the airbrush was implemented using an automated system with a precision syringe pump, which was mounted on the moving part above the spraying system. The dispensing resolution of the suspension was 0.1 µl. Ink delivery from the syringe to the airbrush, as well as filling the syringe with ink, were carried out through a PTFE tube connected to a steel needle with an inner diameter of 0.8 mm. The suspension was delivered through the needle to the nozzle area, where it was atomized in the air stream (Fig. 1b). When passing through sections of the spraying path where suspension deposition was not required, a function for retracting ink from the needle back into the syringe was implemented to prevent leakage. Before resuming spraying, this volume of suspension was purged back out.

The air supply system for the airbrush consisted of several components: an air compressor (JAS 1203), a pressure regulator, an air valve, and an electronic pressure sensor. The maximum air pressure was 5 atm. An air membrane regulator equipped with a pressure gauge was used to set the pressure at the airbrush inlet. Furthermore, at the start and end of the spraying process, the air supply to the system was controlled by an air solenoid valve, which was operated by a signal from the Arduino board.

An automated CNC platform was used for airbrush positioning. Movement was achieved along two axes using stepper motors. Control was implemented using GRBL firmware installed on an Arduino microcontroller board and the G-code programming language. Generation of the G-code command sequence for moving the airbrush along a specified trajectory and sending the commands to the spraying system was performed using a program written in Python 3.x (utilizing the PySide2 software package). The program's input parameters included the width and length of the spraying area, the number of subdivisions of the spraying area along both axes, and the traverse speed.

The movement trajectory within a single iteration is shown in Fig. 2. In the first stage, spraying was performed along the selected direction; transitioning to an adjacent line was carried out with a two-step offset.

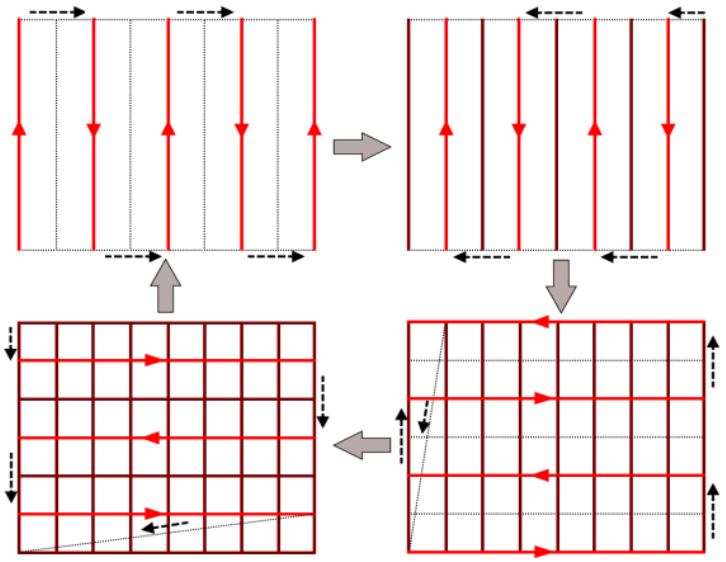

Fig. 2. Airbrush movement trajectory schematic.

The implemented trajectory enabled spraying onto a rectangular GDL with a high degree of uniformity. The step offset value was selected based on several factors: minimizing the size of areas with low catalyst quantity, preventing overlap of adjacent spray lines and the formation of areas with excess liquid catalyst suspension, and generally corresponded to the spray spot size. To elucidate the influence of spraying parameters on the layer architecture and performance, a fixed catalyst loading of 1 mg·cm^{-2} was maintained on the substrate surface.

The use of perforated plate as the surface material for a vacuum platform is widely employed for fixing polymer films, and several commercially available models exist. Compared to perforated plate, porous titanium does not have this drawback, as the distance between adjacent pores is extremely small, and air evacuation occurs uniformly across the entire surface of the vacuum platform.

The model of the vacuum platform is shown in Fig. 3 and consists of a porous titanium plate and a plastic mold with numerous stiffening ribs to prevent deformation of the titanium plate. To reduce the surface roughness of the plate, grinding was performed. A silicon gasket was used for membrane sealing.

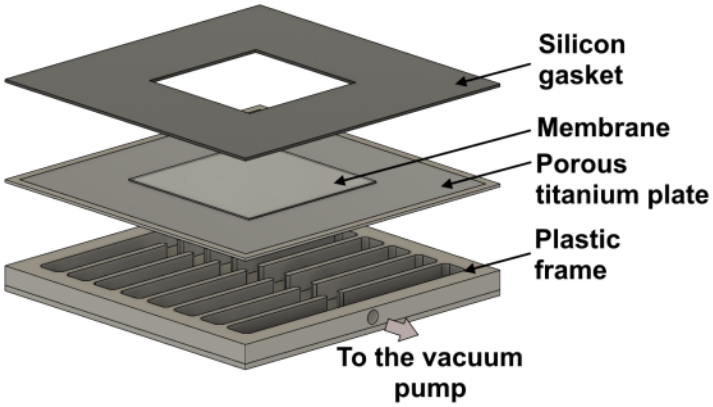

Fig. 3. Image of the vacuum platform components.

The vacuum platform was connected to a Welch 2522C-02 (USA) vacuum pump and was capable of achieving a pressure of up to 200 millibar.

2.3. Microscopy. The uniformity of the formed films was evaluated using a Levenhuk DTX 90 digital optical microscope (USA) with 10 − 300× magnification.

The electrode surface morphology was studied using a Helios Nanolab 600 (ThermoFisher Scientific, USA) scanning electron microscope (SEM). The images were acquired using ETD

(Everhardt-Thornley Detector) and TLD (Through-the-lens detector) secondary electron detectors at an accelerating voltage of 2 kV and a beam current of 86 pA.

SEM images were processed using ImageJ software [39]. The thickness of the catalyst layer was determined by taking measurements at several points across the sample. The reported value represents the average of these measurements, and the corresponding standard deviation was calculated.

2.4. Electrochemical studies. Recording i-V curves allows for evaluating the efficiency and determining the influence of external operating conditions on the stability of a PEMFC of a given composition. A CorrTest CS350 electrochemical workstation (CorrTest Instruments, China) was used for the measurements. The i-V curves were recorded in the voltage range from 0.9 to 0.1 V, with a scan rate of $\upsilon = 5$ mV·s^{-1}. The cell temperature was 30 °C. A PEM water electrolyzer was used as the source of reactants (H_2 and O_2) with the gas flow regulated by the electric current value. The single fuel cell consisted of smoothed bipolar plates and a titanium mesh for gas distribution and water management. The flow rates of the supplied gases were 80 ml·min^{-1} for hydrogen and 40 ml·min^{-1} for oxygen. Reactant gases were humidified to approximately 70% relative humidity using a temperature-controlled water bubbler system. The reactant gases were supplied at a pressure of 1 atm to both the anode and cathode. The reproducibility was assessed from a minimum of three measurements per CL sample. The reproducibility was assessed from a minimum of three measurements per CL sample. The results showed high repeatability, with a deviation of approximately 5 %.

The electrochemical impedance spectroscopy method was used in the study of PEMFCs to determine and separate the contributions of ohmic and polarization losses. Impedance spectra were measured using a CorrTest CS350 electrochemical workstation with an impedance module (CorrTest Instruments, China). The frequency range studied was 0.1 – 10^5 Hz with a signal amplitude of 20 mV at a DC voltage of 0.5 V. The experimental data were described using an equivalent circuit, $R_M(R_A, CPE_A)(R_C, CPE_C)$, where R_M, R_A, R_C – represent the contributions of the ohmic resistance of the PEM and the polarization resistances of the anode and cathode, respectively. CPE_A and CPE_C – are constant phase elements corresponding to the anode and cathode, connected in parallel to their respective resistances. Transport losses under the used operating conditions were negligible and were not accounted for in the applied model.

3. Results and Discussion

3.1. Investigation of the influence of catalyst ink composition on the spraying process

3.1.1. Investigation of the influence of solvent type. A solution of DI water and alcohol was used as the solvent for preparing the catalyst ink suspension. Water is necessary to prevent spontaneous ignition of the electrocatalyst upon interaction with alcohol, as well as to vary the drying rate and viscosity of the resulting catalyst ink. The amount of water required to prevent ignition was at least 20 wt.% in the solution. The addition of water also helped reduce the settling rate and agglomeration of electrocatalyst particles. The use of alcohol is necessary to reduce the drying time of the catalyst suspension and for the effective homogenization of the electrocatalyst.

Isopropanol and 1-butanol were considered as alcohols. Butanol has a significantly higher viscosity compared to isopropanol (33.79 mPa·s >> 2.43 mPa·s), but also a longer drying time. To evaluate the influence of the alcohol on the quality of the CL, two types of catalyst inks were prepared, one with isopropanol and one with 1-butanol. The resulting suspensions were applied to the surface of a glassy carbon electrode using a micropipette and dried at room temperature (Fig. 4).

The use of 1-butanol led to the formation of a "coffee ring stain" during drying because, despite the high viscosity of the alcohol and the lower mobility of the electrocatalyst particles, solvent evaporation occurred over a prolonged period. In the case of isopropanol, the film exhibited a high degree of uniformity due to its faster drying rate. Consequently, isopropanol was selected as the alcohol for further investigation.

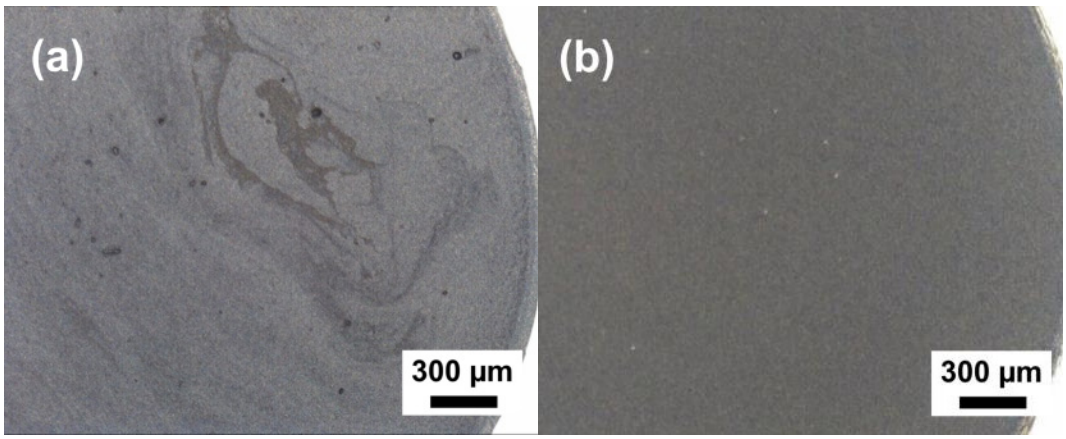

Fig. 4. Optical micrograph (100x magnification) of the CL surface on a glassy carbon electrode obtained from a suspension with 1-butanol (a) and isopropanol (b).

To evaluate the effect of the water-to-alcohol ratio in the solution, CL samples were prepared by spraying 1 ml of suspension with water-to-alcohol ratios of 1:4, 1:2, and 1:1.

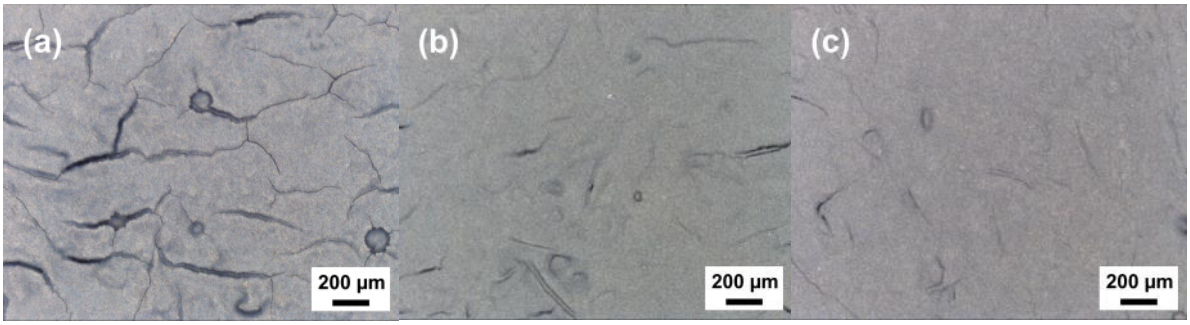

Fig. 5. Optical micrograph (250x magnification) of the CL surface corresponding to suspensions with water-to-alcohol ratios of 1:4 (a), 1:2 (b), and 1:1 (c).

Fig. 5 shows that with the addition of more water, due to slower drying, the catalyst suspension flows into the cracks of the microporous layer, resulting in fewer cracks on the CL surface. A more uniform CL surface may promote better membrane adhesion; however, the penetration of catalyst into the cracks leads to a reduction of its quantity in the membrane-adjacent region, meaning a lower effective loading, and necessitates the application of more catalyst to achieve the target loading (~1 $mg \cdot cm^{-2}$).

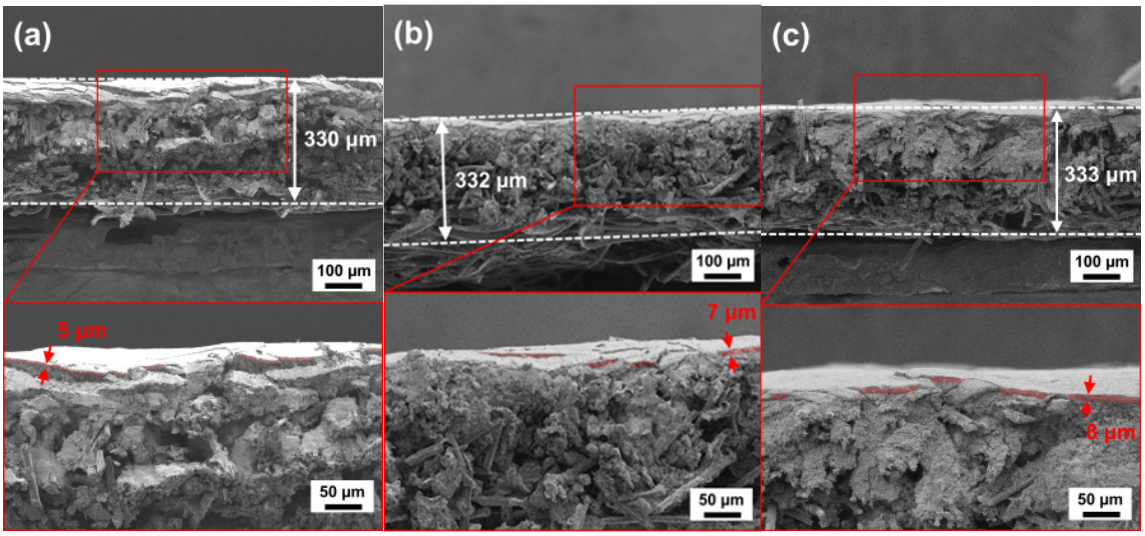

Fig. 6. SEM images of the cross-section of the GDL with a CL corresponding to suspensions with water-to-alcohol ratios of 1:4 (a), 1:2 (b), and 1:1 (c). The CL cross-section is highlighted in red.

Furthermore, the presence of cracks in the fabricated CL may impair PEMFC stability. This degradation mechanism can include the propensity of these cracks to propagate during membrane swelling and shrinkage under humidity cycling, and the accelerated corrosion of the carbon support at these vulnerable sites within the cathode [4,19]. It should also be noted that cracks and large pores can adversely affect water transport within the porous electrode, potentially leading to accelerated MEA failure during operation under non-ideal conditions [6].

SEM images of the GDL and CL cross-sections in Fig. 6 show high uniformity in CL thickness across the examined area, indicating a uniform spraying process. Since increasing the water content in the solution leads to the penetration of the catalyst suspension deeper into the GDL volume, the CL thickness also increases. With a water-to-alcohol ratio of 1:4, the CL thickness was 4.8 ± 0.4 μm, while with ratios of 1:2 and 1:1, it was 6.9 ± 0.5 μm and 8.0 ± 0.3 μm, respectively.

3.1.2. Investigation of the influence of catalyst fraction in the suspension. The amount of catalyst in the suspension was selected considering several factors: the formation of agglomerates at high suspension density and the spraying duration required to achieve the target loading density. With a high amount of catalyst in the suspension (more than 10 mg·ml^{-1}) clogging of the airbrush's ink supply needle occurred. Using low catalyst concentrations in the solution is possible for achieving lower loading densities with a fixed suspension volume. Furthermore, reducing the catalyst concentration in the suspension does not affect either the spraying process or the quality of the CL surface (Fig. 7).

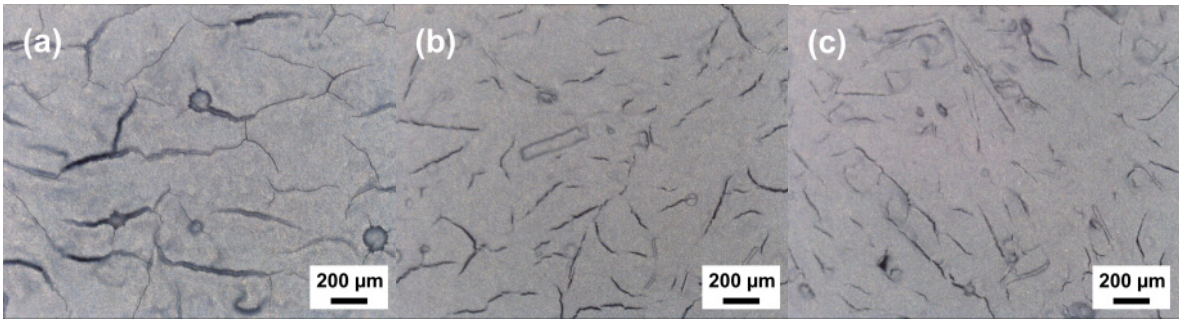

Fig. 7. Optical micrograph (250x magnification) of the CL surface corresponding to suspensions with catalyst concentrations of 10 (a), 5 (b), and 2.5 mg·ml^{-1} (c).

3.1.3. Investigation of the effect of Nafion® ionomer addition. According to studies [40,41] the optimal Nafion® ionomer content in the CL is approximately 20 wt.%. This ionomer content, when applied using the spraying technique, yields an optimal CL architecture, which is free of large ionomer agglomerates, possesses a well-developed triple-phase boundary, and provides sufficient porosity for reagent transport [42,43]. However, the presence of ionomer in the suspension significantly increases its viscosity and adhesion upon drying, which also raises the possibility of nozzle clogging. Therefore, after each spraying session, a cleaning procedure of the catalyst ink supply components with alcohol was required. In addition to increasing the risk of clogging, the presence of ionomer leads to increased catalyst adhesion to the walls of the catalyst suspension container, resulting in additional losses.

3.1.4. Optimal catalyst ink composition. As a result of the conducted research, an optimal composition for the catalyst ink was determined, enabling the production of CLs with stable morphology and high result reproducibility, as well as the absence of clogs in the ink delivery system. The suspension composition is presented in Table 1.

Table 1. Optimal catalyst suspension composition.

Parameter	Value
Alcohol	Isopropanol
Volume fraction of water in alcohol solution	Not less than 20% and not more than 50%

Catalyst concentration in suspension	Not more than 10 mg·ml^{-1}
Ionomer fraction in CL	20 wt.%

3.2. Investigation of the influence of airbrush traverse speed, sprayed substance flow rate, and drying temperature of catalyst compositions on the thickness and quality of the resulting catalyst layer

3.2.1. Investigation of the influence of catalyst ink flow rate. The ink flow rate during spraying was calculated as the ratio of the sprayed volume of catalyst suspension to the total trajectory length. The flow rate was varied by changing the number of iterations, i.e., by altering the total trajectory length. The flow rate value was selected based on minimizing the spraying time, preventing spillage of the suspension on the GDL surface, and reducing the drying time (Fig. 8).

Fig. 8. Image of the spray track at different flow rate values: 54 (left), 81 (center), and 108 µl·min^{-1} (right).

Considering the length and width of the sprayed suspension spot (Fig. 8), at a flow rate of 108 µl·min^{-1} the drying time was excessively long, leading to the accumulation of liquid suspension on the surface and its penetration into the GDL. At a flow rate of 81 µl·min^{-1} the spot length was shorter; however, due to the spot width being larger than the offset size, track overlap occurred at the edges of the spraying area, also resulting in liquid suspension accumulation. At a flow rate of 54 µl·min^{-1} overlap of adjacent track lines did not occur, therefore this value was selected as the maximum.

Fig. 9 shows that with an increase in flow rate, penetration of the catalyst suspension deeper into the GDL also occurred, and the CL thickness increased from 4.8 ± 0.4 µm at a flow rate of 54 µl·min^{-1}, to 10.2 ± 1.0 µm at a flow rate of 108 µl·min^{-1}.

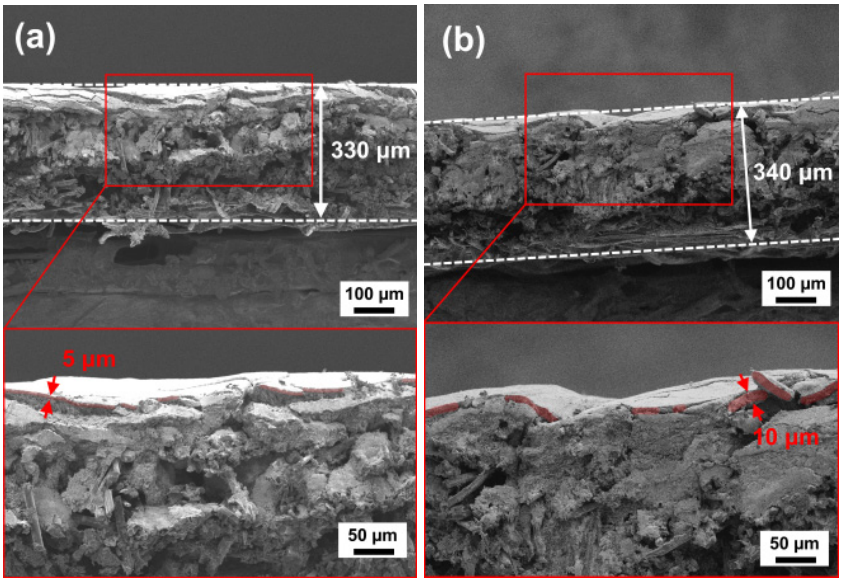

Fig. 9. SEM images of the cross-section of a GDL with a CL, corresponding to a flow rate of 54 µl·min^{-1} (a) and 108 µl·min^{-1} (b). The CL cross-section is highlighted in red.

3.2.2. Investigation of the influence of catalyst ink drying temperature. When studying the temperature effect on the CL, the maximum temperature of the heating element was selected based on the thermal stability of the device housing components and was set to 60 °C (the temperature was recorded at the GDL surface). The drying temperature during spraying affected both the surface morphology and the thickness of the CL. As the temperature increased, the number of cracks increased, which is explained by less penetration of the catalyst suspension into the GDL cracks at higher temperatures due to the higher drying rate. Consequently, the surface structure of the CL at a heater temperature of 60 °C replicated the GDL surface morphology more closely than at a temperature of 40 °C (Fig. 10).

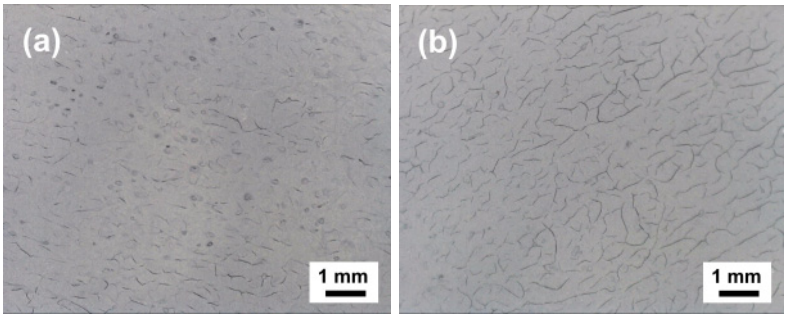

Fig. 10. Optical micrographs (70x magnification) of the CL surface sprayed at a temperature of 40 °C (a) and 60 °C (b).

In addition to macroscopic changes in the surface structure, differences in the size and quantity of pores on the CL surface were observed at smaller scales. For CLs obtained by drying without heating, the size and quantity of surface pores were minimal, whereas increasing the temperature significantly increased porosity, as evidenced by the increase in the number of dark zones in Fig. 11.

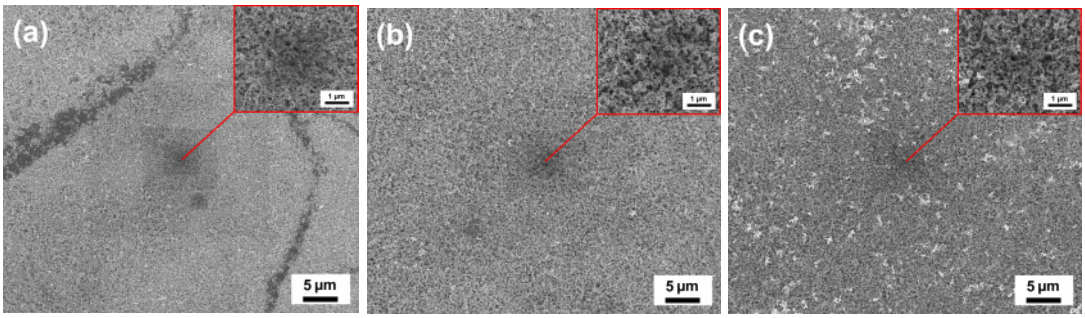

Fig. 11. SEM images of the CL surface sprayed without heating (a), at a temperature of 40 °C (b), and at 60 °C (c).

For the sample without heating, the area corresponding to pores constituted 20% of the total image area; for the sample heated to 40 °C, the pore fraction was 26%; and at 60 °C, it reached a maximum of 37%. Furthermore, at a drying temperature of 60 °C, many bright inclusions are observed, which represent ionomer films. Their presence can be explained by the higher degree of ionomer molecule adhesion at elevated temperatures, leading to the formation of agglomerates on the CL surface. Ionomer particles on the layer surface can block pores, hindering gas supply and reducing the efficiency of the electrochemical device [42]. Additionally, a decrease in ionomer uniformity within the CL can cause performance and durability losses due to a reduction in the triple-phase boundary area and deterioration of mechanical properties [43].

Increasing the drying temperature led to a decrease in CL thickness due to reduced penetration of the suspension into the GDL volume. Without heating, the observed thickness of the CL was 4.8 ± 0.4 µm; at a heating temperature of 40 °C – 4.0 ± 0.3 µm; and at 60 °C – 2.9 ± 0.5 µm (Fig. 12).

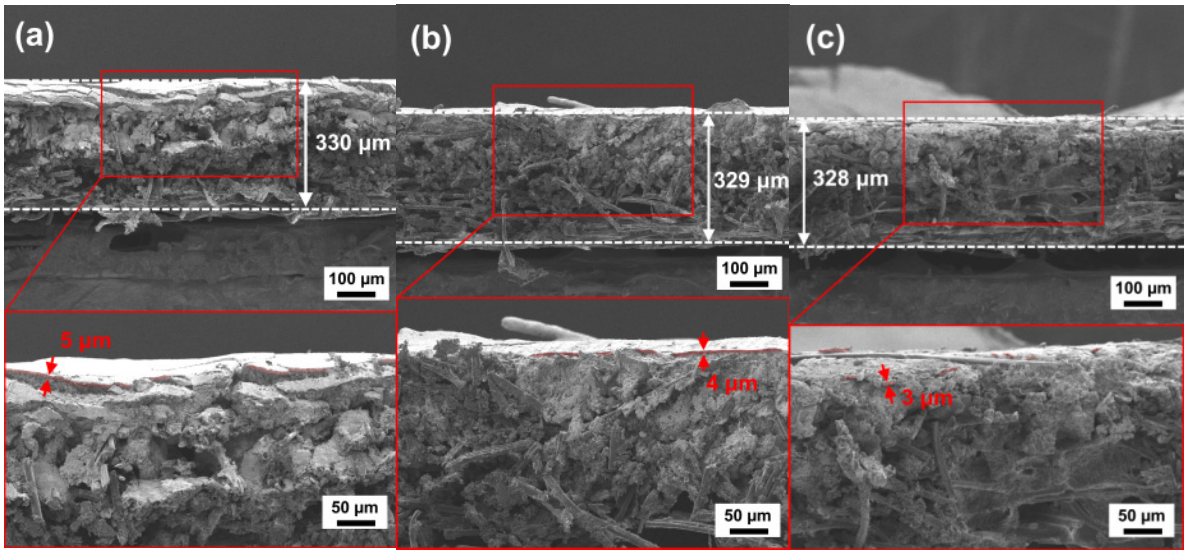

Fig. 12. SEM images of the cross-section of the GDL with a CL sprayed without heating (a), at a temperature of 40 °C (b), and at 60 °C (c). The CL cross-section is highlighted in red.

Thus, considering the discussed factors, the most optimal drying temperature for the catalyst suspension is approximately 40 °C.

The spraying speed was varied by increasing the rotation speed of the stepper motors in the positioning system, while simultaneously increasing the feed rate of the catalyst suspension to maintain a constant flow. The acceleration of the stepper motors was kept unchanged. Given the constant flow and acceleration, the change in speed did not affect the CL thickness. The maximum airbrush traverse speed was limited by the power of the stepper motors and was 4000 mm/min.

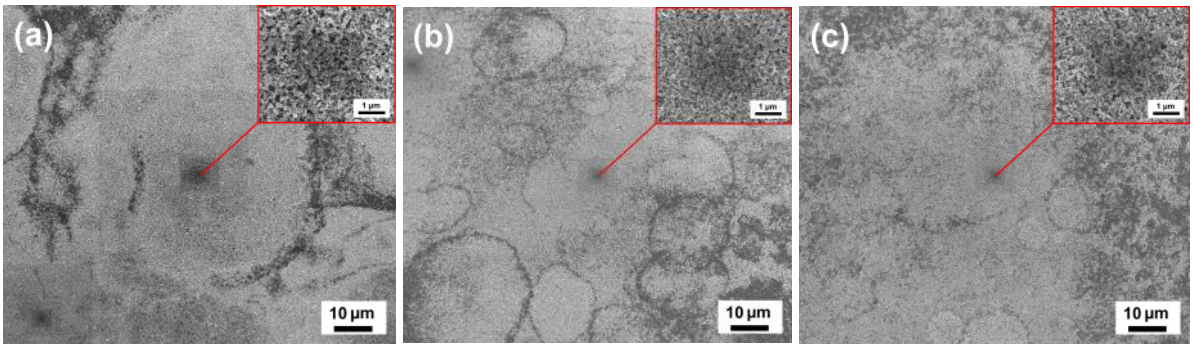

Fig. 13. SEM images of the CL surface at airbrush traverse speeds of 1000 (a), 2000 (b), and 4000 mm·min^{-1} (c).

The surface structure of the CL depending on the traverse speed is presented in Fig. 13. In the SEM images corresponding to speeds of 2000 and 4000 mm·min^{-1}, dark circular spots are observed, formed during the drying of suspension droplets. As the speed increases, the size of these areas decreases, which may indicate a reduction in the size of the sprayed droplets due to more efficient liquid dispersion in the air stream. Furthermore, at higher speeds, the CL surface becomes less uniform, reflected by the presence of many dark areas. Thus, when increasing the airbrush traverse speed to reduce spraying time, the negative impact of this parameter on the final uniformity of the CL surface should be considered.

3.2.4. Optimal spraying parameters. As a result of the research conducted, a set of optimal spraying parameters was determined, enabling the production of high-quality CLs with uniform thickness. The list of parameters is presented in Table 2.

Table 2. Optimal catalyst suspension composition.

Parameter	Value

Flow rate	Not more than 54 µl·min^{-1}
Drying temperature	40 °C
Maximum airbrush traverse speed (for achieving uniform CL surface)	1000 mm·min^{-1}
Maximum airbrush traverse speed (for minimizing spraying time)	4000 mm·min^{-1}

3.3. Investigation of the influence of catalyst suspension drying parameters on the properties of the PEM

3.3.1. Investigation of the influence of heater temperature magnitude. According to study [44], the method of depositing the electrocatalyst directly onto the surface of the PEM has several differences compared to the process of depositing onto the electrode surface. Spraying onto the membrane allows for better performance of electrochemical devices and reduced catalyst losses, which occur due to the penetration of the catalyst suspension into the porous electrode layer. However, this method can lead to negative consequences such as deformation due to swelling and membrane degradation as a result of its interaction with alcohol, even to the point of forming pinholes. Such effects can occur when there is an excess of solvent on the membrane surface during spraying. To prevent the accumulation of solvents, external heat sources are used to increase the drying rate of alcohol.

To investigate the influence of the heater temperature on the drying process of the catalyst suspension on the membrane surface and to account for the size and position of the infrared heater relative to the airbrush nozzle, a temperature map of the substrate surface was constructed. The resulting distribution is presented in Fig. 14.

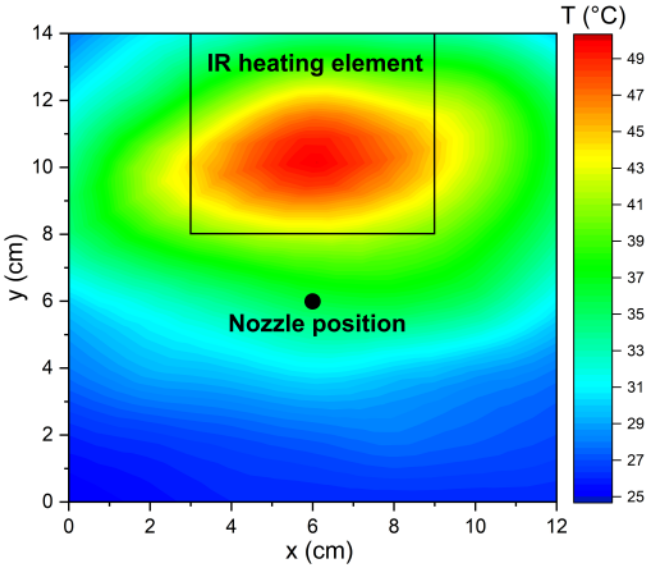

Fig. 14. Temperature map (°C) of the spraying area surface. The thermocouple temperature was 40 °C. The position of the airbrush nozzle is indicated by a circular symbol; the position of the IR heater is highlighted by a rectangle.

Based on the obtained temperature distribution, it is evident that the area of maximum temperature (50 °C) is located above the position of the airbrush nozzle, which is explained by the inability to place the heater directly above the nozzle. Nevertheless, the small spraying area, combined with the placement of the IR heater on the moving part of the spraying system, ensures a more uniform temperature distribution across the substrate surface.

The influence of temperature on the quality of the deposited layer was assessed based on the surface morphology of the resulting MEA. Checks for pinholes in the membrane were conducted within a PEMFC test cell by measuring the open-circuit voltage (OCV). Spraying was performed on

both sides of the membrane with the IR heater turned off, as well as at temperatures in the spraying area of 40 °C and 50 °C. The remaining spraying parameters for all samples were the previously obtained optimal values listed in Table 3.

Table 3. Optimal parameters for spraying the CL onto the PEM.

Parameter	Value
Flow rate	54 µl·min^{-1}
Catalyst suspension composition	4 mg catalyst (Pt^{40}/C^{10}), 1.6 ml isopropyl alcohol, 0.4 ml water, 0.1 mg ionomer
Maximum airbrush traverse speed (for achieving uniform CL surface)	1000 mm·min^{-1}
Spraying area	2 × 2 cm^2
Distance between adjacent spray lines	2 mm
Membrane	Nafion® 212

When the IR heater was turned off, the suspension dried solely due to the air flow from the airbrush; however, the drying rate in this case was insufficient, leading to membrane deformation at the edges of the spraying area (Fig. 15). Such deformations can result in less tight adhesion between the catalyst layer and the gas diffusion layer surface, leading to poor conductivity between the layers.

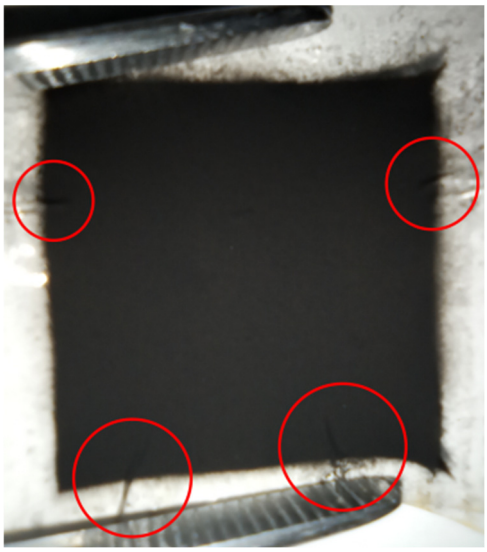

Fig. 15. Image of the membrane surface with the deposited catalyst layer without heating. Membrane defects are outlined in red.

When the heater temperature was increased to 40 °C, more intensive evaporation of the suspension solvent occurred, which prevented the formation of sample surface warping (Fig. 16 left). A sample was also obtained at a heating temperature of 50 °C; in this case, a homogeneous and uniform catalyst layer was similarly obtained (Fig. 16 right).

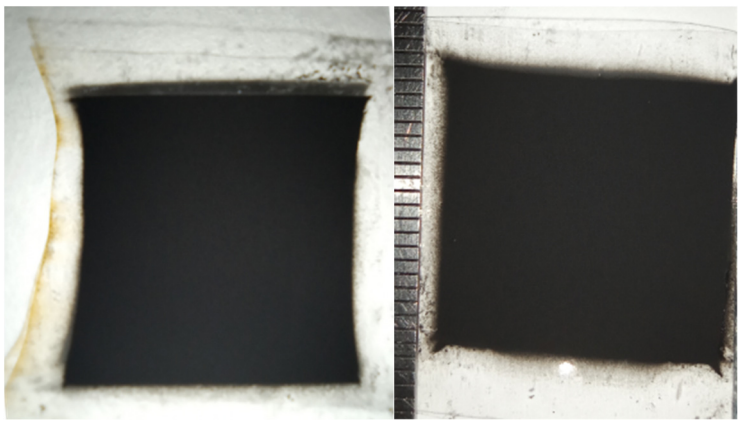

Fig. 16. Image of the membrane surface with the deposited catalyst layer at a heater temperature of 40 °C (left) and 50 °C (right).

Since at higher heater temperatures (above 60 °C) excessive heating of the airbrush nozzle and drying of the suspension directly inside the delivery system are possible, experiments at higher heating temperatures were not conducted.

The obtained MEAs were tested within a fuel cell to check for pinholes in the membrane. The OCV values recorded during testing are presented in Table 4. The low OCV value for the sample obtained without heating indicates possible membrane damage and reactant crossover. At higher temperatures with a fixed flow rate of 54 $\mu l \cdot min^{-1}$, the OCV is close to the value of 0.9 V, characteristic of an intact PEM under standard conditions.

Table 4. OCV values for MEA samples.

Heating Temperature (°C)	OCV Value (V)
No heating	0.73
40	0.88
50	0.91

3.3.2. Investigation of the influence of catalyst suspension flow rate. In addition to increasing the heater temperature, the formation of excess solvent on the membrane surface can be prevented by reducing the amount of suspension sprayed per unit length of the trajectory. To optimize the flow rate, spraying was conducted not only at 54 $\mu l \cdot min^{-1}$, but also at flow rates of 108 $\mu l \cdot min^{-1}$, 81 $\mu l \cdot min^{-1}$ and 69 $\mu l \cdot min^{-1}$ with a heater temperature of 50 °C.

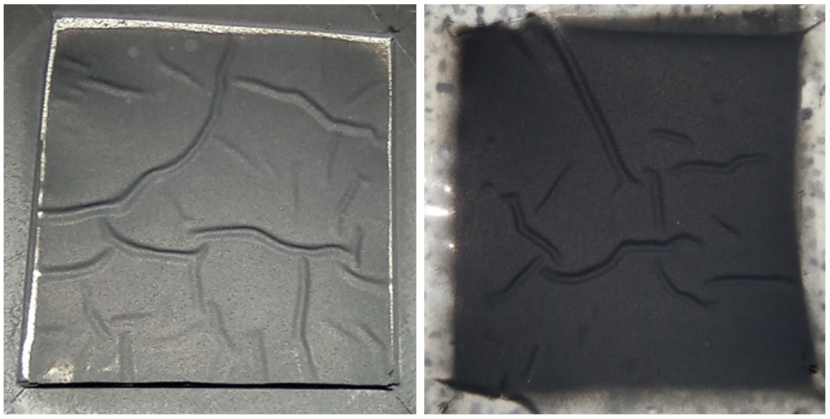

Fig. 17. Image of the membrane surface with the deposited catalyst layer at flow rates of 108 (left) and 81 $\mu l \cdot min^{-1}$ (right).

At flow rates of 108 and 81 $\mu l \cdot min^{-1}$ the entire membrane surface deformed significantly due to an excess of suspension. This caused non-uniform swelling and wrinkle formation which persisted after the CL formation. Fig. 17 shows the surface of the obtained membrane samples with the

deposited catalyst layer. The reduction in the number of defects with decreasing flow rate indicates the positive effect of lowering this parameter on the quality of the resulting MEAs.

When the flow rate was reduced to 69 µl·min^{-1}, the number and size of defects became insignificant. An image of the resulting catalyst layer is presented in Fig. 18.

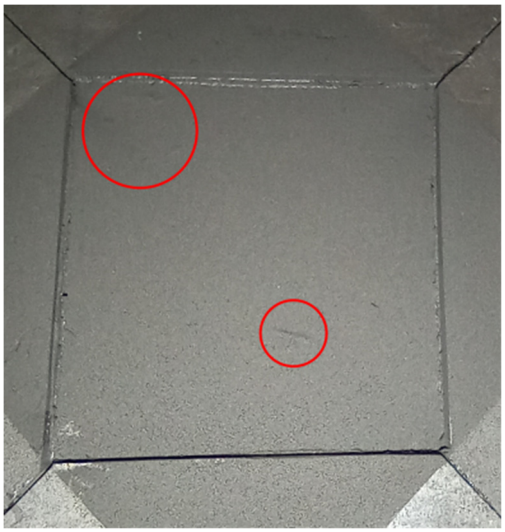

Fig. 18. Image of the membrane surface with the deposited catalyst layer at a flow rate of 69 µl·min^{-1}. Membrane defects are outlined in red.

The OCV values recorded during testing are presented in Table 5. At flow rates of 108 and 81 µl·min^{-1}, the OCV has a low value, which may indicate possible formation of pinholes in the membrane due to its dissolution in the alcohol, which leads to gas crossover, or a low contact area between the gas diffusion layer and the catalyst layer. At lower flow rates and with almost no defects on the surface, the MEA samples demonstrate high OCV values.

Table 5. OCV values for MEA samples.

Suspension Flow Rate (µl·min^{-1})	OCV Value (V)
108	0.67
81	0.75
69	0.90
54	0.91

As a result of the conducted research, a set of optimal spraying parameters was determined, enabling the production of high-quality CLs without membrane damage or surface defect formation. The optimal parameters are a heating temperature of 40–50 °C and a suspension flow rate up to 69 µl·min^{-1}.

3.4. Electrochemical studies of the obtained layers

3.4.1. Spraying parameters for the samples. The parameters of the automated spraying system used for depositing the catalyst layer onto Nafion® 212 membranes are presented in Table 6. The catalyst loading density was 1 mg·cm^{-2}.

Table 6. Parameters for spraying catalyst suspension onto the membrane surface for various samples.

Sample	Suspension Drying Temperature (°C)	Flow Rate (µl·min^{-1})
MEA1	50	54
MEA2	40	54

MEA3	No heating	54
MEA4	50	69
Manual spraying (PEM)	40 – 50	-

Since the I-V curve of a PEMFC depends on the CL composition, samples with the same amount of electrocatalyst (1 mg·cm^{-2}) and ionomer in the layer (20 wt.%) were selected for the study. The previously determined optimal flow rate value of 54 µl·min^{-1} was chosen. The parameters of the automated spraying system for depositing the catalyst layer onto the GDL surface are presented in Table 7.

Table 7. Parameters for spraying catalyst suspension onto the GDL surface for various samples.

Sample	Volume Fraction of Water in Catalyst Ink (%)	Suspension Drying Temperature (°C)	Airbrush Traverse Speed (mm·min^{-1})
MEA5	20	No heating	1000
MEA6	20	No heating	4000
MEA7	20	40	1000
MEA8	33	No heating	1000
MEA9	50	No heating	1000
Manual spraying (GDL)	20	40 – 50	-

3.4.2. Electrochemical studies. The obtained i-V curves for MEA samples with different CL deposition methods are presented in Fig. 19.

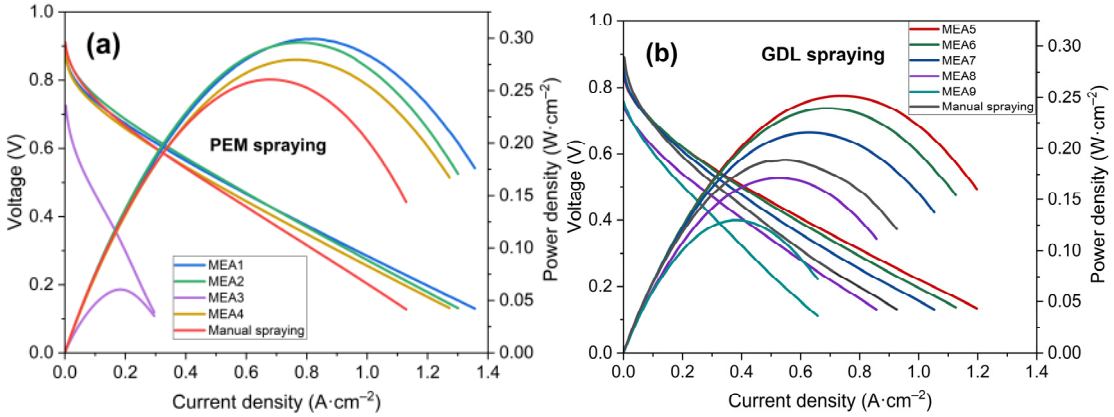

Fig. 19. I-V curves and power density of MEA samples obtained by spraying onto the membrane (a, left) and onto the GDL (b, right). Scan rate 20 mV·s^{-1}.

Samples obtained by depositing the catalyst onto the membrane surface (Fig. 19 a) exhibit higher efficiency compared to samples obtained by depositing the catalyst onto the GDL (Fig. 19 b). The maximum specific power density values for the PEMFC were 0.30 ± 0.02 W·cm^{-2} for MEA1 and MEA2, and 0.28 ± 0.02 W·cm^{-2} for MEA4, respectively. For manual spraying onto the membrane, this value was 0.26 ± 0.01 W·cm^{-2}. Thus, the use of the manual spraying method allows for the production of MEAs with comparable efficiency; the uniformity of CL deposition on the PEM has a minor effect. However, the significant decrease in specific power for sample MEA3, obtained without heating, indicates probable membrane damage (formation of pinholes) due to prolonged exposure to alcohol combined with the presence of a pressure differential during vacuum fixation.

In the case of spraying onto the GDL, the highest maximum specific power density values correspond to samples MEA5 and MEA6, reaching 0.25 ± 0.01 W·cm^{-2} and 0.24 ± 0.01 W·cm^{-2},

respectively. The slight decrease in efficiency for the sample sprayed at four times the airbrush traverse speed demonstrates the minor influence of this parameter on layer uniformity. Furthermore, the absence of additional heating during the fabrication of these samples did not negatively impact efficiency due to the high evaporation rate of alcohol in the catalyst ink under air flow. Conversely, when heating was used, the compaction of the CL, as shown in Fig. 12, led to reduced porosity due to accelerated drying of the catalyst ink. This decreased the accessibility of active sites to reactants and resulted in a lower maximum specific power density for MEA7 of 0.22 ± 0.01 $W \cdot cm^{-2}$. In the case of manual spraying with heating, the maximum specific power density was significantly lower at 0.19 ± 0.01 $W \cdot cm^{-2}$, indicating a greater contribution of CL uniformity to performance when spraying onto the GDL compared to spraying onto the PEM.

The study of MEAs fabricated using catalyst inks with a higher water content showed that the lower drying rate of the catalyst ink promotes its penetration into deeper pores of the GDL, consequently disrupting the CL morphology, adversely affecting its porosity and triple-phase boundaries. Thus, for samples MEA8 and MEA9, a decrease in maximum specific power density to 0.17 ± 0.01 $W \cdot cm^{-2}$ and 0.13 ± 0.01 $W \cdot cm^{-2}$, respectively, was observed.

Nyquist plots were obtained, presented in Fig. 20, and the model parameters were determined using the provided equivalent circuit.

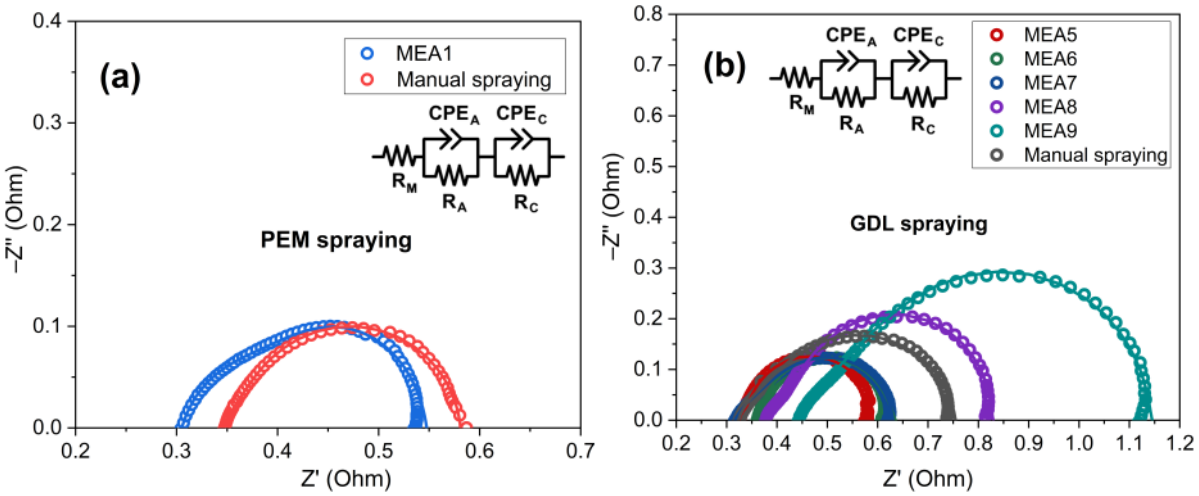

Fig. 20. Nyquist plots of PEMFC samples obtained by spraying onto the membrane (a, left) and onto the GDL (b, right). Cell voltage 0.5 V.

For samples with catalyst ink deposited on the membrane, a decrease in membrane resistance is shown in the case of automated spraying: 0.31 Ohm for MEA1 versus 0.35 Ohm for manual spraying. This effect can be explained by damage to the PEM by the alcohol in the case of excess catalyst ink deposition, which is more likely with manual spraying. The total polarization resistance for these samples was comparable: 0.23 Ohm and 0.24 Ohm for manual spraying and MEA1, respectively.

The results of impedance spectroscopy for the samples with spraying onto the GDL correspond to the voltammetry results – the lowest ohmic and polarization resistances are observed for MEA5 (R_M = 0.33 Ohm, R_A+R_C = 0.27 Ohm) and MEA6 (R_M = 0.36 Ohm, R_A+R_C = 0.28 Ohm). The lowest ohmic resistance value for MEA7 (0.31 Ohm) indicates the best contact between the CL and the PEM; however, an increase in polarization resistance (0.31 Ohm) is observed due to reduced accessibility of the electrocatalyst's active sites resulting from the increased density of the CL. Samples MEA8 and MEA9 show an increase in polarization resistance (0.45 Ohm and 0.70 Ohm, respectively), due to the disrupted structure of the CL. A significant increase in ohmic resistance is also observed for MEA9 (R_M = 0.44 Ohm), which may indicate increased contact resistance at the CL/PEM interface. For manual spraying, an increase in polarization resistance to 0.43 Ohm is also shown, yet the ohmic resistance was 0.33 Ohm, indicating a relatively low contribution of CL surface non-uniformity to the CL/PEM contact resistance.

Based on the data obtained, the higher efficiency of MEAs with catalyst ink deposited on the PEM surface has been demonstrated; however, in this case, prolonged contact of the solvent with the membrane can lead to the formation of defects in the membrane, which necessitates the application of heating.

Conclusions

The work presents a comparative analysis of the influence of spraying parameters on the properties of the resulting CLs when spraying onto PEM and GDL surfaces. It is shown that the optimal spraying parameters for the CL differ significantly depending on the substrate type (PEM or GDL). Furthermore, the use of an automated spraying system enables an increase in the specific power of MEAs compared to the manual method: by 15% when spraying onto the PEM and by 32% when spraying onto the GDL.

It has been established that for forming the CL on the GDL surface, the uniformity of deposition and the drying rate of the catalyst ink have a key influence. The optimal parameters for this substrate are low water content in the ink (no more than 20%) and the absence of external heating, whereas the airbrush traverse speed has a less significant impact on the quality of the resulting CL.

In the case of spraying onto the PEM, the most critical parameter is the drying temperature. The spraying process for this substrate is characterized by a maximum airbrush traverse speed that is four times lower compared to deposition onto the GDL. However, the higher adhesion of the CL to the PEM compensates for this drawback, providing a 20% higher efficiency of the final MEAs.

Thus, it can be concluded that the spraying process onto the PEM imposes higher requirements on the deposition parameters, is characterized by a lower speed, and is associated with the risk of membrane damage; however, the use of an automated system allows for the minimization of these risks. In turn, spraying onto the GDL is a less demanding and faster process, but its efficiency is largely determined by the optimization of the catalyst ink composition to form a CL with optimal morphology.

Declaration of Competing Interest

The authors declare that they have no known competing financial interests or personal relationships that could have appeared to influence the work reported in this paper.

Data availability

No data was used for the research described in the article.

Funding

This research was funded by the Russian Science Foundation, grant number 25-19-00281, https://rscf.ru/project/25-19-00281/.

Acknowledgments

The authors gratefully acknowledge the support provided by the "Fund for Assistance to Small Innovative Enterprises in Science and Technology" through the "UMNIK" program for the development of the spraying system.

Conflict of Interest

The authors announced that there are no conflicts of interest regarding this current work

References

1. Grineva D.E., Mensharapov R.M., Ivanova N.A., Spasov D.D., Sinyakov M.V., Aliyev A.Sh., Fateev V.N. Hydrogen-supported decarbonization of automotive industry: from ICE through

hybrids to FC vehicles. *International Journal of Hydrogen Energy?* 2025, **Vol. 192,** 152238**.** DOI: 10.1016/j.ijhydene.2025.152238.
2. Zhao C., Yuan S., Cheng X., Zheng Z., Liu J., Yin J., Shen Sh., Yan X., Zhang J. The effect of catalyst layer design on catalyst utilization in PEMFC studied via stochastic reconstruction method. *Energy and AI.* 2023, **Vol. 13,** 100245. DOI: 10.1016/j.egyai.2023.100245.
3. Zhou Y., Kang J., Chen B., Zheng W., Zhang C., Ming P., Pan F., Wang J., Li B. Formation mechanism and morphology control of cracks in PEMFC catalyst layer during fabrication process: A review. *Advances in Colloid and Interface Science*, 2025, **Vol. 340,** 103468. DOI: 10.1016/j.cis.2025.103468.
4. Lee C., Komini B.S., Patterson B.M., Reeves K.S., Yu H., Cullen D.A., Mukundan R., Borup L.R., Spendelow J.S. Effect of Engineered Cracks in Catalyst Layers on PEMFC Catalyst Layer Durability. *Journal of The Electrochemical Society*, 2024, **Vol. 171,** 014502. DOI: 10.1149/1945-7111/ad1b7b.
5. Ivanova N.A., Alekseeva O.K., Fateev V.N., Shapir B.L., Spasov D.D., Nikitin S.M., Presnyakov M.Yu., Kolobylina N.N., Soloviev M.A., Mikhalev A.I., Grigoriev S.A. Activity and durability of electrocatalytic layers with low platinum loading prepared by magnetron sputtering onto gas diffusion electrodes. *International Journal of Hydrogen Energy,* 2019, **Vol. 44**, p. 29529–29536. DOI: 10.1016/j.ijhydene.2019.04.096.
6. Mensharapov R.M., Ivanova N.A., Spasov D.D., Bakirov A.V., Fateev V.N. PEMFC performance at nonstandard operating conditions: A review. *International Journal of Hydrogen Energy*, 2024, **Vol. 96**, p. 664–679. DOI: 10.1016/j.ijhydene.2024.11.395.
7. Zasypkina A.A., Ivanova N.A., Spasov D.D., Mensharapov R.M., Alekseeva O.K., Vorobyeva E.A., Kukueva E.V., Fateev V.N. Electrode with a carbon nanotube array for a proton exchange membrane fuel cell. *Inorganics*, 2023, **Vol. 11(5)**, 219. DOI: 10.3390/inorganics11050219
8. Ott S., Du F., Luna M.L., Dao T.A., Cuenya B.R., Orfanidi A., Strasser P. Understanding the performance increase of catalysts supported on N-functionalized carbon in PEMFC catalyst layers. *Journal of The Electrochemical Society*, 2022, **Vol. 169,** 054520. DOI: 10.1149/1945-7111/ac6e4d.
9. Dou S., Hao L., Liu H. Effects of carbon aggregates and ionomer distribution on the performance of PEM fuel cell catalyst layer: A pore-scale study. *Renewable Energy*, 2023, **Vol. 217,** 119254. DOI: 10.1016/j.renene.2023.119254.
10. Liu Y., Cai X., Lu J., Du A., Lin R. Pt Active Site Density Optimization of the Catalyst Layer for an Ultralow-Pt-Loading PEMFC. *Energy Fuels*, 2024, **Vol. 38**, p. 21423–21431. DOI: 10.1021/acs.energyfuels.4c03749.
11. Wan Y., Qiu D., Yi P., Peng L., Lai X. Design and optimization of gradient wettability pore structure of adaptive PEM fuel cell cathode catalyst layer. *Applied Energy*, 2022, **Vol. 312,** 118723. DOI: 10.1016/j.apenergy.2022.118723.
12. Ivanova N.A., Sinyakov M.V., Grineva D.E., Trigub A.L., Chumakov R.G., Kolyshkin N.A., Oparin S.K., Kudryashov V.V., Zhang C., Spasov D.D. Composition–structure–activity–durability relationship of carbon-supported Pt-modifier hetero-clusters for the oxygen reduction reaction. *Journal of Power Sources*, 2026, **Vol. 694,** 241312. DOI: 10.1016/j.jpowsour.2026.241312.
13. Grineva D.E., Mensharapov R.M, Sinyakov M.V., Spasov D.D. Development of impurity-tolerant electrocatalysts for durable proton exchange membrane fuel cells: A review. *Chimica Techno Acta,* 2026, **Vol. 13,** 9942. DOI: 10.15826/chimtech.9942.
14. Mensharapov R.M., Bakirov A.V., Grineva D.G., Sinyakov M.V., Fateev V.N., Spasov D.D. Structural degradation of Nafion® and SiO2/Nafion® PEMs under thermal cycling: Ionic domain fragmentation and proton conductivity loss. *Chimica Techno Acta*, 2026, **Vol. 13,** 10047. DOI: 10.15826/chimtech.10047.
15. Mensharapov R.M., Spasov D.D., Ivanova N.A., Zasypkina A.A., Smirnov S.A., Grigoriev S.A. Screening of carbon-Supported platinum electrocatalysts using Frumkin adsorption isotherms. *Inorganics,* 2023, **Vol. 11,** 103. DOI: 10.3390/inorganics11030103.

16. Mensharapov R.M., Ivanova N.A., Zasypkina A.A., Spasov D.D., Sinyakov M.V., Grigoriev S.A., Fateev V.N. Model study of CNT-based PEMFCs' electrocatalytic layers. *Catalysts*, 2022, **Vol. 12,** 1227. DOI: 10.3390/catal12101227.
17. Xie M., Chu T., Wang T., Wan K., Yang D., Li B., Ming P., Zhang C. Preparation, Performance and Challenges of Catalyst Layer for Proton Exchange Membrane Fuel Cell. *Membranes*, 2021, **Vol. 11,** 879. DOI: 10.3390/membranes11110879.
18. Xie Z., Yu S., Yang G., Li K., Ding L., Wang W., Zhang F.-Y. Optimization of catalyst-coated membranes for enhancing performance in proton exchange membrane electrolyzer cells. *International Journal of Hydrogen Energy*, 2021, **Vol. 46**, p. 1155–1162. DOI: 10.1016/j.ijhydene.2020.09.239.
19. Arcot M.P., Cronin M., Fowler M., Pritzker M. Morphological characteristics of catalyst layer defects in catalyst-coated membranes in PEM fuel cells. *Electrochem*., 2023, **Vol. 4**, p. 1–20. DOI: 10.3390/electrochem4010001.
20. Vinodh R., Palanivel T., Kalanur S.S., Pollet B.G. Recent advancements in catalyst coated membranes for water electrolysis: a critical review. *Energy Advances*, 2024, **Vol. 3**, p. 1144–1166. DOI: 10.1039/d4ya00143e.
21. Quarz P., Zimmerer N., Steck A.-M., Scharfer P., Schabel W. Carbon Nanotubes (CNT) as an additive towards crack-free catalyst coated membranes (CCM). *International Journal of Hydrogen Energy*, 2024, **Vol. 57**, p. 789–797. DOI: 10.1016/j.ijhydene.2024.01.049.
22. Turtayeva Z., Xu F., Dillet J., Mozet K., Peignier R., Celzard A., Maranzana G. Manufacturing catalyst-coated membranes by ultrasonic spray deposition for PEMFC: Identification of key parameters and their impact on PEMFC performance. *International Journal of Hydrogen Energy*, 2022, **Vol. 47**, p. 16165–16178. DOI: 10.1016/j.ijhydene.2022.03.043.
23. Lee J., Lee H., Kim J.H., Pham T.A., Jang S., Kim S.M. Investigation of optimized spraying process for directly coated electrode in polymer electrolyte membrane fuel cell. *Journal of Industrial and Engineering Chemistry*, 2024, **Vol. 132,** p. 474–481. DOI:10.1016/j.jiec.2023.11.041.
24. Ma M., Shen L.X., Liu J., Xu B., Zhang Y., Zhao L., Wang Z.B. Recent advances in Pt catalysts and membrane electrode assemblies fabrication for proton exchange membrane fuel cells. *Rare Metals*, 2024, **Vol. 43**, p. 4198-4221. DOI: 10.1007/s12598-024-02698-6.
25. Talukdar K., Morawietz T., Sarkezi-Selsky P., Yezerska K., Sergeev O., Heger J.-F., Jahnke Th., Gazdzicki P., Friedrich K.A. Exploring critical parameters of electrode fabrication in polymer electrolyte membrane fuel cells. *Journal of Power Sources*, 2022, **Vol. 540,** 231638. DOI: 10.1016/j.jpowsour.2022.231638.
26. Han C., Bian T., Proskurin A., Senin P., Kong W., Chen D. Minimizing the local oxygen transport resistance in PEMEC via CCM drying process optimization. *International Journal of Hydrogen Energy*, 2025, **Vol. 124**, p. 263–270. DOI: 10.1016/j.ijhydene.2025.04.036.
27. Ney L., Seidl N., Singh R., Schneider P., Stross D., Göppentin D., Tepner S., Klingele M., Keding R. Screen Printing Catalyst Inks With Enhanced Process Stability for PEM Fuel Cell Production. *Fuel Cells*, 2025, **Vol. 25,** e202400158. DOI: 10.1002/fuce.202400158.
28. Mendoza Peña K.J., Tsuji R., Fukuda T., Tanabe M., Ito S. Optimization of Three-Component Solvent Systems for Scalable Screen-Printed PEM Fuel Cells. *ACS Applied Engineering Materials*, 2025, **Vol. 3(6)**, p. 1522–1532. DOI: 10.1021/acsaenm.5c00097.
29. Ney L., Hog J., Singh R., Göttlicher N., Schneider P., Tepner S., Klingele M., Keding R., Clement F., Groos U. Challenges of fabricating catalyst layers for PEM fuel cells using flatbed screen printing. *Journal of Coatings Technology and Research*, 2023, **Vol. 20**, p. 73–86. DOI: 10.1007/s11998-022-00710-1.
30. Jeong S., Kwon O., Yoo H., Kim J., Choi H., So Y., Park J., Lee J., Jeong Y., Park T. High platinum utilization for proton exchange membrane fuel cells via low-temperature substrate sputtering on acid-treated carbon nanotube sheet. *Chemical Engineering Journal*, 2023, **Vol. 466,** 143135. DOI: 10.1016/j.cej.2023.143135.

31. Yang Y., Yuan S., Liu J., Zhang Z., Lu T. Effect of catalyst ink particle size on the structure of the catalyst layer and electrical performance in the process of ultrasonic spray manufacturing PEMFCs. *Energy*, 2024, **Vol. 294,** 130605. DOI: 10.1016/j.energy.2024.130605.
32. Li H., Zhao H., Tao B., Xu G., Gu S., Wang G., Chang H. Pt-based oxygen reduction reaction catalysts in proton exchange membrane fuel cells: controllable preparation and structural design of catalytic layer. *Nanomaterials*, 2022, **Vol. 12,** 4173. DOI: 10.3390/nano12234173.
33. Du S., Guan S., Mehrazi S., Zhou F., Pan M., Zhang R., Chuang P.-Y. A., Sui P.-Ch. Effect of dispersion method and catalyst on the crack morphology and performance of catalyst layer of PEMFC. *Journal of The Electrochemical Society*, 2021, **Vol. 168,** 114506. DOI: 10.1149/1945-7111/ac3598.
34. Cooper C.D., Burk J.J., Taylor C.P., Buratto S.K. Ultra-low Pt loading catalyst layers prepared by pulse electrochemical deposition for PEM fuel cells. *Journal of Applied Electrochemistry*, 2017, **Vol. 47**, p. 699–709. DOI: 10.1007/s10800-017-1071-4.
35. Chun H., Kim Y., Chae H., Lee M., Han B., Kim M., Choi H., Hur J.W., Kim H.-S., Ok J.G. Facile Airbrush Fabrication of Gas Diffusion Layers Comprising Fine-Patterned Hydrophobic Double-Layer and Hydrophilic Channel for Improved Water Removal in Polymer Electrolyte Membrane Fuel Cells. *International Journal of Precision Engineering and Manufacturing-Green Technology,* 2021, **Vol. 8**, p. 1461-1469. DOI: 10.1007/s40684-020-00254-y.
36. Yurko Y, Elbaz L. The effect of membrane electrode assembly methods on the performance in fuel cells. *Electrochimica Acta*, 2021, **Vol. 389,** 138676. DOI: 10.1016/j.electacta.2021.138676.
37. Su H., Jao T.-C., Barron O., Pollet B.G., Pasupathi S. Low platinum loading for high temperature proton exchange membrane fuel cell developed by ultrasonic spray coating technique. *Journal of Power Sources*, 2014, **Vol. 267**, p. 155–159. DOI: 10.1016/j.jpowsour.2014.05.086.
38. Mensharapov R.M., Ivanova N.A., Spasov D.D., Kukueva E.V., Zasypkina A.A., Seregina E.A., Grigoriev S.A., Fateev V.N. Carbon-Supported Pt-SnO_2 Catalysts for Oxygen Reduction Reaction over a Wide Temperature Range: Rotating Disk Electrode Study. *Catalysts*, 2021, **Vol. 11,** 1469. DOI: 10.3390/catal11121469.
39. Schneider C.A., Rasband W.S., Eliceiri K.W. NIH Image to ImageJ: 25 years of image analysis. *Nature Methods*, 2012, **Vol. 9**, p. 671–675. DOI: 10.1038/nmeth.2089.
40. Chen G.-Y., Wang C., Lei Y.-J., Zhang J., Mao Z., Mao Z.-Q., Guo J.-W., Li J., Ouyang M. Gradient design of Pt/C ratio and Nafion content in cathode catalyst layer of PEMFCs. *International Journal of Hydrogen Energy*, 2017, **Vol. 42**, p. 29960–29965. DOI:10.1016/j.ijhydene.2017.06.229.
41. Kim K.-H., Kim H.-J., Lee K.-Y., Jang J.H., Lee S.-Y., Cho E., Oh I.-H., Lim T.-H. Effect of Nafion® gradient in dual catalyst layer on proton exchange membrane fuel cell performance. *International Journal of Hydrogen Energy*, 2008, **Vol. 33**, p. 2783–2789. DOI:10.1016/j.ijhydene.2008.03.015.
42. Dou S., Hao L., Wang Q., Liu H. Effects of agglomerate structure and operating humidity on the catalyst layer performance of PEM fuel cells. *Applied Energy*, 2024, **Vol. 355,** 122211. DOI: 10.1016/j.apenergy.2023.122211.
43. Guo Y., Pan F., Chen W., Ding Z., Yang D., Li B., Ming P., Zhang C. The Controllable Design of Catalyst Inks to Enhance PEMFC Performance: A Review. *Electrochemical Energy Reviews*, 2021, **Vol. 4**, p. 67–100. DOI: 10.1007/s41918-020-00083-2.
44. Lim B.H., Majlan E.H., Tajuddin A., Husaini T., Wan Daud W.R., Mohd Radzuan N.A., Haque M.A. Comparison of catalyst-coated membranes and catalyst-coated substrate for PEMFC membrane electrode assembly: A review. *Chinese Journal of Chemical Engineering*, 2021, **Vol. 33**, p. 1–16. DOI: 10.1016/j.cjche.2020.07.044.